University of Texas Rio Grande Valley

ScholarWorks @ UTRGV

Physics and Astronomy Faculty Publications and Presentations

College of Sciences

5-6-2002

Equilibrium shapes of flat knots

Ralf Metzler

Andreas Hanke
The University of Texas Rio Grande Valley

Paul G. Dommersnes

Yacov Kantor
Tel Aviv University

Mehran Kardar

Follow this and additional works at: https://scholarworks.utrgv.edu/pa_fac

 Part of the Astrophysics and Astronomy Commons

Recommended Citation

Ralf Metzler, et. al., (2002) Equilibrium shapes of flat knots.Physical Review Letters88:181881011. DOI: http://doi.org/10.1103/PhysRevLett.88.188101

This Article is brought to you for free and open access by the College of Sciences at ScholarWorks @ UTRGV. It has been accepted for inclusion in Physics and Astronomy Faculty Publications and Presentations by an authorized administrator of ScholarWorks @ UTRGV. For more information, please contact justin.white@utrgv.edu, william.flores01@utrgv.edu.

Equilibrium Shapes of Flat Knots

Ralf Metzler,[1] Andreas Hanke,[1] Paul G. Dommersnes,[1] Yacov Kantor,[2,1] and Mehran Kardar[1,3]

[1]*Department of Physics, Massachusetts Institute of Technology, Cambridge, Massachusetts 02139*
[2]*School of Physics and Astronomy, Sackler Faculty of Exact Sciences, Tel Aviv University, Tel Aviv 69978, Israel*
[3]*Institute for Theoretical Physics, University of California at Santa Barbara, Santa Barbara, California 93106*

(Received 12 October 2001; published 19 April 2002)

We study the equilibrium shapes of prime and composite knots confined to two dimensions. Using scaling arguments we show that, due to self-avoiding effects, the topological details of prime knots are localized on a small portion of the larger ring polymer. Within this region, the original knot configuration can assume a hierarchy of contracted shapes, the dominating one given by just one small loop. This hierarchy is investigated in detail for the flat trefoil knot, and corroborated by Monte Carlo simulations.

DOI: 10.1103/PhysRevLett.88.188101 PACS numbers: 87.15.Ya, 02.10.Kn, 82.35.Pq, 87.15.Aa

The static and dynamic behavior of single polymer chains, such as DNA, and multichain systems like gels and rubbers, is strongly influenced by knots and permanent entanglements [1,2]. Topological constraints are created with probability one during the polymerization of long closed chains [3,4]; more generally, knots and entanglements are a ubiquitous element of higher molecular multichain melts and solutions. This has profound consequences, reaching far into biology and chemistry. For instance, knots in DNA impede the separation of the two strands of the double helix during transcription, and therefore the access to the genetic code [5]. Chemically, even single closed polymers may exhibit quite different properties if they have different topology [6]. In the nanosciences, recent experimental techniques allow *single* polymer molecules (with fixed topology) to be probed and manipulated [7]. These tools provide impetus for the theoretical understanding of the behavior of macromolecules under topological constraints. However, analytical studies, such as the statistical mechanics of a knotted polymer, are difficult since topological constraints require knowledge of the complete shape of the curve. Such global constraints are hard to implement, and a complete statistical mechanical description of knots remains unattained; compare, for instance, Ref. [8].

The mathematical discipline of knot theory provides invariants for the classification of knots [2,9]. In particular, different knots can be distinguished by their *projections* onto a 2D plane, keeping track of crossings according to which segment passes on top of another [2]. By a sequence of so-called Reidemeister moves [2], which leave the topology unchanged, the number of crossings can be reduced to a minimum, which is a simple topological invariant [2]. For instance, in Fig. 1 we depict the minimal projection of the trefoil knot, classified as 3_1, with its 3 crossings. Such quasi-2D projections, which we call *flat knots,* can be physically realized by compressing originally 3D knots by forces normal to the projection plane. Examples include polymers adsorbed on a surface or membrane by electrostatic or other adhesive forces [10]; or confined between parallel walls. In these cases the flat polymer knot can still equilibrate in 2D. Another experimental realization comes from Ref. [11], in which macroscopic knotted chains are flattened by gravity onto a vibrating plane. The equilibrium shapes, and their scaling properties, of such flat knots are studied in this paper. Flat knots have the additional advantage of being easy to image by microscopy. They are also more amenable to numeric studies than their 3D counterparts, and have in fact been already studied in Refs. [12,13].

There is growing numerical evidence that prime knots are *tight* in the sense that the topologically entangled region is statistically likely to be localized on a small portion of the longer chain [13–15], consistent with the findings of Ref. [4] in which the optimal size in random knotting is studied. Indirect numerical evidence of this was originally obtained by simulations indicating that the radius of gyration of a long polygon in 3D is asymptotically independent of its knot type; while the presence of the knot increases the number of configurations by a factor related to the number of positions of the tight region around the remaining loop [15]. Simulations of 2D polygons in Ref. [13] provide quite convincing visual evidence of localized knot regions. In this paper, we *quantify the tightness of flat knots,* using scaling arguments to obtain the power law size distributions for a hierarchy of possible equilibrium shapes. For the trefoil, Fig. 1 shows this hierarchy of shapes and the corresponding exponents for the distribution of knot size.

To get a feeling for the entropic origin of tight shapes, consider first a simple flat, once-twisted ring of length L with one crossing. This figure-eight shape consists of two loops of variable lengths ℓ and $L - \ell$, while the orientation of the crossing is irrelevant. In this sense, the crossing can be replaced with a vertex with four outgoing legs, resulting in the network $\mathcal{G}_1$ depicted in Fig. 1. In fact, we can more generally consider a sliding ring, or slip link [16], holding close together two points of the chain to create the figure-eight shape in d dimensions. Without self-avoiding constraints (ideal chains), the number of configurations $\omega_1(\ell, L)$ scales as [1,17]

$$\omega_1(\ell, L) \sim \mu^L \ell^{-d/2} (L - \ell)^{-d/2}, \qquad (1)$$

where, on a lattice, μ is the effective connectivity constant

 © 2002 The American Physical Society

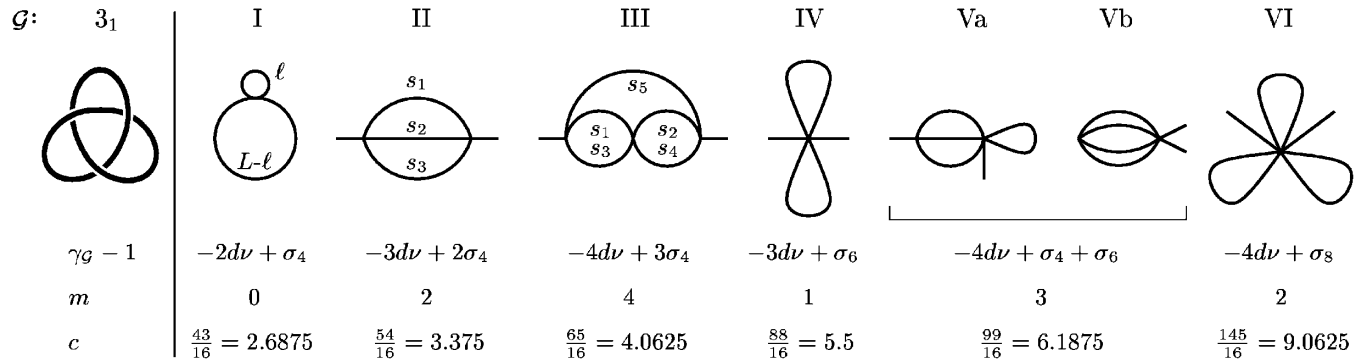

FIG. 1. Standard minimal projection of the trefoil knot 3_1, followed by its different possible contractions, arranged according to higher scaling orders. The uncontracted trefoil geometry is found at position III of the hierarchy. At I, the figure-eight structure is drawn. The diagrams II–VI show the multiply connected knot region of total length $\ell = \sum_{i=1}^{\mathcal{N}-1} s_i$ where the protruding legs indicate the outgoing large loop of length $s_\mathcal{N} = L - \ell$. Below the individual contractions, we include the network exponents $\gamma_\mathcal{G}$, the number m of independent integrations, and the exponents c defined via the PDF, $p(\ell) \sim \ell^{-c}$.

for Gaussian random walks. The average loop size is $\langle \ell \rangle = \int_a^{L-a} d\ell\, \ell \omega_1(\ell, L) / \int_a^{L-a} d\ell\, \omega_1(\ell, L) = L/2$ due to symmetry, where a is a short-distance cutoff set by the lattice constant. However, the corresponding probability density function (PDF) is strongly peaked at $\ell = 0$ and $\ell = L$, and a *typical* shape consists of one tight and one large loop. In $d = 2$, the mean size of the smaller loop, $\langle \ell \rangle_< \sim L/|\ln(a/L)|$, is still rather large. It is instructive to compare to higher dimensions: one has *weak localization,* $\langle \ell \rangle_< \sim a^{1/2} L^{1/2}$, in $d = 3$, and *strong localization,* $\langle \ell \rangle_< \sim a$, in $d > 4$. Thus, for ideal chains, tightness of the smaller loop is more pronounced in higher dimensions.

To include self-avoiding interactions, we use results for general polymer networks obtained by Duplantier [18], and in Refs. [19,20]: In a network $\mathcal{G}$ consisting of $\mathcal{N}$ chain segments of lengths $s_1, \ldots, s_\mathcal{N}$ and total length $L = \sum_{i=1}^{\mathcal{N}} s_i$, the number of configurations $\omega_\mathcal{G}$ scales as [21]

$$\omega_\mathcal{G}(s_1, \ldots, s_\mathcal{N}) = \mu^L s_\mathcal{N}^{\gamma_\mathcal{G}-1} \mathcal{Y}_\mathcal{G}\left(\frac{s_1}{s_\mathcal{N}}, \ldots, \frac{s_{\mathcal{N}-1}}{s_\mathcal{N}}\right), \quad (2)$$

where $\mathcal{Y}_\mathcal{G}$ is a scaling function, and μ is the effective connectivity constant for self-avoiding walks. The exponent $\gamma_\mathcal{G}$ is given by $\gamma_\mathcal{G} = 1 - d\nu\mathcal{L} + \sum_{N\geq 1} n_N \sigma_N$, where ν is the swelling exponent, $\mathcal{L}$ is the number of independent loops, n_N is the number of vertices with N outgoing legs, and σ_N is an exponent associated with such a vertex. In $d = 2$, $\sigma_N = (2 - N)(9N + 2)/64$ [18].

The network $\mathcal{G}_\mathrm{I}$ corresponds to the parameters $\mathcal{N} = 2$, $\mathcal{L} = 2$, $n_4 = 1$, $s_1 = \ell$, and $s_2 = L - \ell$. By virtue of Eq. (2), the number of configurations of $\mathcal{G}_\mathrm{I}$ with fixed ℓ follows the scaling form

$$\omega_\mathrm{I}(\ell, L) = \mu^L (L - \ell)^{\gamma_\mathrm{I}-1} \mathcal{X}_\mathrm{I}\left(\tfrac{\ell}{L-\ell}\right), \quad (3)$$

where $\gamma_\mathrm{I} = 1 - 2d\nu + \sigma_4$. In the limit $\ell \ll L$, $\omega_\mathrm{I}(\ell, L)$ should reduce to the number $\omega_\mathrm{crw}(L) \sim \mu^L L^{-d\nu}$ of *closed random walks* of length L which start and end at a given point in space [17,22]. This implies $\mathcal{X}_\mathrm{I}(x) \sim x^{\gamma_\mathrm{I}-1+d\nu}$ as $x \to 0$, such that

$$\omega_\mathrm{I}(\ell, L) \sim \mu^L (L - \ell)^{-d\nu} \ell^{-c}, \qquad \ell \ll L, \quad (4)$$

where $c = -(\gamma_\mathrm{I} - 1 + d\nu) = d\nu - \sigma_4$. Using $\sigma_4 = -19/16$ and $\nu = 3/4$ in $d = 2$, we find $c = 43/16 = 2.6875$. In $d = 3$, $\sigma_4 \approx -0.48$ and $\nu \approx 0.588$, so that $c \approx 2.24$ [19,22]. In both cases the result $c > 2$ implies that the loop of length ℓ is strongly localized in the sense defined above. This justifies the *a priori* assumption $\ell \ll L$, and makes the analysis self-consistent. Note that for self-avoiding chains, in $d = 2$ the localization is even *stronger* than in $d = 3$, in contrast to the corresponding trend for ideal chains. We performed Monte Carlo (MC) simulations of the 2D figure-eight structure $\mathcal{G}_\mathrm{I}$, in which the slip link was represented by three tethered beads enforcing the sliding pair contact such that the loops cannot fully retract (see Fig. 2). We used a

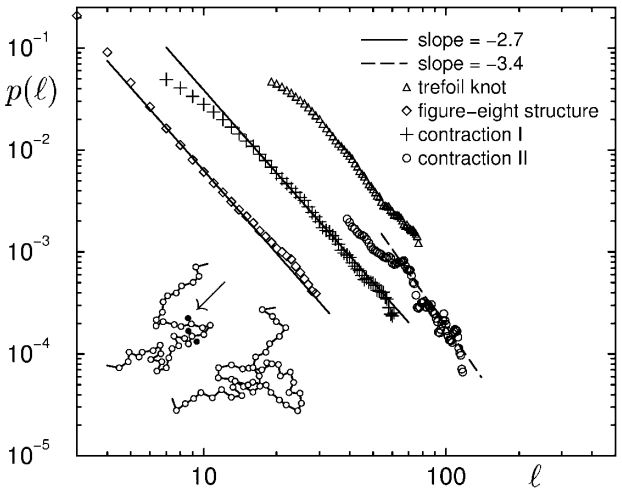

FIG. 2. Power law tails in PDFs for the size ℓ of tight segments: As defined in the figure, we show results for the smaller loop in a figure-eight structure, the overall size of the trefoil knot, as well as the two leading contractions of the latter. The insets show typical configurations of the small loop for a 2D figure-eight (the arrow points to the slip link consisting of three tethered beads), and the knot region of the flat trefoil.

2D hard-core bead-and-tether chain with 256 monomers, starting off from a symmetric initial condition with $\ell = L/2$. Self-crossings were prevented by keeping a maximum bead-to-bead distance of 1.38 times the bead diameter, and a maximum step length of 0.15 times the bead diameter. We estimate the simulation time to be well above the Rouse relaxation time [1] of the chain. As shown in Fig. 2, the size distribution for the small loop can be fitted to a power law with exponent $c = 2.7 \pm 0.1$ [23], in good agreement to the above prediction.

For the figure-eight shape $\mathcal{G}_{\mathrm{I}}$, the probability for the size of each loop is peaked at $\ell \to 0$ and $\ell \to L$. For more complicated structures, the joint probability to find the individual segments with given lengths s_i is expected to peak at the edges of the higher-dimensional configuration hyperspace. Some analysis is necessary to find the optimal shapes; as presented here for the simplest nontrivial knot, the (flat) trefoil knot 3_1 shown in Fig. 1 [24]. Each of the three crossings is replaced with a vertex with four outgoing legs, and the resulting network is assumed to separate into a large loop and a multiply connected region which includes the vertices. Let $\ell = \sum_{i=1}^{5} s_i$ be the total length of all segments contained in the multiply connected knot region (see Fig. 1, position III). Accordingly, the length of the large loop is $L - \ell$. In the limit $\ell \ll L$, the number of configurations of the network $\mathcal{G}_{\mathrm{III}}$ can be derived in a similar way as above, yielding

$$\omega'_{\mathrm{III}} \sim \mu^L (L - \ell)^{-d\nu} \ell^{\gamma_{\mathrm{III}} - 1 + d\nu} \mathcal{W}\left(\frac{s_1}{\ell}, \frac{s_2}{\ell}, \frac{s_3}{\ell}, \frac{s_4}{\ell}\right), \tag{5}$$

where $\gamma_{\mathrm{III}} = 1 - 4d\nu + 3\sigma_4$ and $\mathcal{W}$ is a scaling function. The prime on ω_{III} indicates that the segment lengths s_i are kept fixed. In order to obtain the number of individual configurations $\omega_{\mathrm{III}}(\ell, L)$ for the case of the flat trefoil, where only the total length ℓ is fixed and the different segments fluctuate in length, we integrate ω'_{III} over all distributions of lengths s_i under the constraint $\sum_{i=1}^{5} s_i = \ell$. This leads to the result

$$\omega_{\mathrm{III}}(\ell, L) \sim \mu^L (L - \ell)^{-d\nu} \ell^{-c}, \tag{6}$$

with $c = -(\gamma_{\mathrm{III}} - 1 + d\nu) - m$, where $m = 4$ corresponds to the number of independent integrations over s_i. Thus, $c = 3d\nu - 3\sigma_4 - 4 = \frac{65}{16}$ (see Fig. 1, position III).

However, some care is necessary in performing these integrations, since the scaling function $\mathcal{W}$ in Eq. (5) may exhibit nonintegrable singularities if one or more of its arguments tend to 0 or 1. The geometries corresponding to these limits (edges of the configuration hyperspace) represent *contractions* of the original trefoil network $\mathcal{G}_{\mathrm{III}}$ in the sense that the length of one or more of the segments s_i is of the order of the short-distance cutoff a. If such a short segment connects different vertices, they cannot be resolved on larger length scales, but melt into a single, new vertex, in the context of our scaling analysis [25]. Thus, each contraction corresponds to a different network $\mathcal{G}$, which may contain a vertex with up to eight outgoing legs. For each of these networks, one can calculate the corresponding exponent c in a similar way as above, and using the relations $2\mathcal{N} = \sum_{N\geq 1} N n_N$ and $\mathcal{L} = \sum_{N\geq 1} \frac{1}{2}(N-2) n_N + 1$, we obtain

$$c = 2 + \sum_{N\geq 4} n_N \left[\frac{N}{2}(d\nu - 1) + (|\sigma_N| - d\nu)\right]. \tag{7}$$

Our scaling analysis relies on an expansion in $a/\ell \ll 1$, and the values of c determine a sequence of contractions according to higher orders in a/ℓ: The *smallest* value of c corresponds to the most likely contraction, while the others represent corrections to this leading scaling behavior, and are thus less and less probable (see Fig. 1). To lowest order, the trefoil behaves like a large ring polymer at whose fringe the pointlike knot region is located. At the next level of resolution, it appears contracted to the figure-eight shape $\mathcal{G}_{\mathrm{I}}$. For more accurate data, the higher order shapes II to VII may be found with decreasing probability. Interestingly, the original uncontracted trefoil configuration ranks third in the hierarchy of shapes. Note that the contractions shown in Fig. 1 may occur in different topological variants. For instance, the smaller loop in contraction I could be inside the larger loop. However, this does not make a difference in terms of the scaling analysis.

These predictions were checked by MC simulations with the same conditions as described above, to prevent intersection. The flat trefoil knot was prepared from a symmetric, harmonic 3D representation with 512 monomers, which was collapsed and then kept on a hard wall by the "gravitational" field $V = -k_B T h/h^*$ perpendicular to the wall, where h is the height and h^* was set to 0.3 times the bead diameter [24]. Configurations corresponding to contraction I are then selected by requiring that besides a large loop, they contain only one segment larger than a preset cutoff length (taken to be 5 monomers), and similarly for contraction II. The size distributions for such contractions, as well as for all possible knot shapes are shown in Fig. 2. The tails of the distributions are indeed consistent with the predicted power laws, although the data (especially for contraction II) is too noisy for a definitive statement.

Our scaling results pertain to all flat prime knots. In particular, the dominating contribution for *any* prime knot corresponds to the figure-eight contraction $\mathcal{G}_{\mathrm{I}}$, as Eq. (7) predicts a larger value of the scaling exponent c for any network $\mathcal{G}$ other than $\mathcal{G}_{\mathrm{I}}$. Accordingly, Fig. 3 demonstrates the tightness of the prime knot 8_{19}. Composite knots, however, can maximize the number of configurations by splitting into their prime factors as indicated in Fig. 3 for $3_1\#3_1$. Each prime factor is tight and located at the fringe of one large loop, and accounts for an additional factor of L for the number of configurations, as compared to a ring of length L without a knot. Indeed, this gain in entropy leads to the tightness of knots.

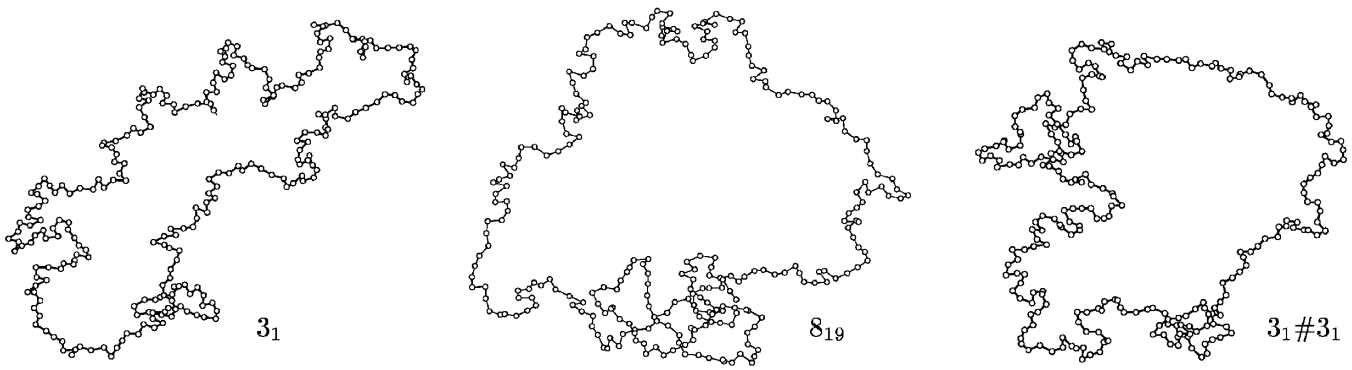

FIG. 3. Typical equilibrium configurations of 256-monomer chains for the trefoil 3_1, the prime knot 8_{19}, and the composite knot $3_1\#3_1$ consisting of two trefoils, in $d = 2$. The initial conditions were symmetric.

In conclusion, we find that the trefoil knot, as well as higher order prime and composite knots, are sharply localized when forced to lie flat. In the most likely shapes, each prime factor is tightened into a loop (a figure-eight contraction). It is natural to speculate that entropic factors also confine 3D knots by power law distributions in size. Direct checks of such behavior are hampered by the difficulty of identifying the knotted region of a 3D curve [14]. One may instead search for indirect signatures of localized knots in higher-order dependencies of gyration radius and other polymeric quantities on length.

R. M. and A. H. acknowledge the DFG, and P. G. D. acknowledges the Research Council of Norway, for financial support. Support from the NSF (DMR-01-18213, PHY99-07949) and the U.S.–Israel BSF (1999-007) is also acknowledged.

[1] P.-G. de Gennes, *Scaling Concepts in Polymer Physics* (Cornell University Press, Ithaca, New York, 1979).
[2] L. H. Kauffman, *Knots and Physics* (World Scientific, Singapore, 2001), 3rd ed.
[3] H. L. Frisch and E. Wasserman, J. Am. Chem. Soc. **83**, 3789 (1961); M. Delbrück, Proc. Symp. Appl. Math. **14**, 55 (1962).
[4] A. Dobay *et al.,* Lett. Math. Phys. **55**, 239 (2001); compare K. Koniaris and M. Muthukumar, Phys. Rev. Lett. **66**, 2211 (1991).
[5] B. Alberts *et al., The Molecular Biology of the Cell* (Garland, New York, 1994).
[6] J.-P. Sauvage and C. Dietrich-Buchecker, *Molecular Catenanes, Rotaxanes, and Knots: A Journey through the World of Molecular Topology* (Wiley-VCH, Weinheim, 1999).
[7] W. E. Moerner and M. Orrit, Science **283**, 1670 (1999); A. van Oudenaarden and J. A. Theriot, Nat. Cell. Biol. **1**, 493 (1999); Y. Arai *et al.,* Nature (London) **399**, 446 (1999).
[8] A. L. Kholodenko and T. A. Vilgis, Phys. Rep. **298**, 254 (1998); A. Yu. Grosberg, Phys. Rev. Lett. **85**, 3858 (2000); M. Otto and T. A. Vilgis, Phys. Rev. Lett. **80**, 881 (1998).
[9] V. I. Arnold, *Topological Invariants of Plane Curves and Caustics* (American Mathematical Society, Providence, RI, 1994); Adv. Sov. Math. **21**, 33 (1994); O. Viro, Am. Math. Soc. Transl. **173**, 231 (1996); S. Tabachnikov, J. Knot Theory Ram. **5**, 531 (1996).
[10] B. Maier and J. O. Rädler, Phys. Rev. Lett. **82**, 1911 (1999).
[11] E. Ben-Naim *et al.,* Phys. Rev. Lett. **86**, 1414 (2001).
[12] A. Grosberg and S. Nechaev, J. Phys. A **25**, 4659 (1992).
[13] E. Guitter and E. Orlandini, J. Phys. A **32**, 1359 (1999).
[14] V. Katritch *et al.,* Phys. Rev. E **61**, 5545 (2000).
[15] E. Orlandini *et al.,* J. Phys. A **31**, 5953 (1998).
[16] M. Doi and S. F. Edwards, J. Chem. Soc. Faraday Trans. 2 **74**, 1802 (1978); R. C. Ball *et al.,* Polymer **22**, 1010 (1981).
[17] Following Refs. [13,15], we consider two configurations as distinct if they cannot be superimposed by translation. This eliminates the degrees of freedom due to translational invariance of the whole structure.
[18] B. Duplantier, Phys. Rev. Lett. **57**, 941 (1986); J. Stat. Phys. **54**, 581 (1989).
[19] L. Schäfer *et al.,* Nucl. Phys. **B374**, 473 (1992).
[20] K. Ohno and K. Binder, J. Phys. (Paris) **49**, 1329 (1988).
[21] This result is valid if the network has at least one vertex with $N \neq 2$ outgoing legs. In contrast, for a simple ring polymer of length L, one has $\omega(L) = \mu^L L^{-d\nu-1}$ [17].
[22] Y. Kafri *et al.,* Phys. Rev. Lett. **85**, 4988 (2000); cond-mat/0108323.
[23] The quoted errors reflect our subjective estimate of possible systematic errors.
[24] We assume that the initial topology is not changed by the formation of additional segments through Reidemeister moves, i.e., twists or the slipping of a part of the chain underneath another. This assumption is corroborated by the evaluation of our simulations, indicating that the gravitational field V sufficiently suppresses the formation of additional segments.
[25] In field theory, this is an example of an operator product expansion; see J. Zinn-Justin, *Quantum Field Theory and Critical Phenomena* (Clarendon Press, Oxford, 1989).